Proxy-Model Comparison for the Eocene-Oligocene Transition in Southern High Latitudes

Emily J. Tibbett[1], Natalie J. Burls[2], David K. Hutchinson[3], Sarah J. Feakins[1]

[1]Department of Earth Science, University of Southern California, Los Angeles, CA, USA

[2]Atmospheric, Oceanic, and Earth Sciences Department, George Mason University, Fairfax, VA, USA

[3]Climate Change Research Centre, University of New South Wales, Sydney, Australia

Key points

- Air temperatures at the margins of the Antarctic continent dropped by 0 to 3°C across the Eocene Oligocene Transition
- Southern high latitude sea surface temperatures mostly cooled by 0 to 3°C.
- Best fit to the proxy surface air temperatures from CO_2-only runs suggest a 25% decrease in pCO_2 across the Eocene-Oligocene Transition

Abstract

The Eocene-Oligocene Transition (EOT) marks the shift from the greenhouse to icehouse conditions at 34 Ma, when a permanent ice sheet developed on Antarctica. Here we compile published proxy temperature records on and around Antarctica for timeslices defined for the late Eocene (40-34Ma) and early Oligocene (34-30 Ma) bracketing the EOT. Compiled proxy records for mean annual sea surface temperature (SST) cool by on average 1°C and land surface mean air temperature (MAT) by 2°C between the timeslices. Proxy data were compared to climate model simulations for each time interval. We use previous climate model simulations representing pre- and post- EOT, typically forced with a halving of pCO_2 – that results in a larger than expected cooling based on proxies for temperature. We scaled the model outputs to identify the magnitude of pCO_2 change needed to drive a commensurate change in temperature to best fit the temperature proxies. Relative to a post-EOT pCO_2 level of 560 ppmv, this temperature scaling approach indicates a 27% decrease in pCO_2, consistent with carbon dioxide proxy reconstructions. These proxy-model intercomparisons show that pCO_2 is the primary driver of declining temperatures across the EOT, and the magnitude of that forcing was likely consistent with the 200 ppmv estimate from the latest pCO_2 proxy compilations.

Plain Language Summary

Antarctica was once a continent with little to no ice on it. Around 34 million years ago Antarctica developed its first permanent ice sheet as temperatures cooled. To evaluate how much cooling occurred on and around Antarctica, we compiled ancient evidence, reported previously in the literature. We then

compared the ancient evidence to climate model experiments which allows us to test cause and effect. Cooling is thought to be caused by a drop in carbon dioxide concentrations in the atmosphere, and we tested how much carbon dioxide levels would need to drop to explain the cooling found. Our estimates are similar to independent evidence from marine organisms for carbon dioxide concentrations.

Keywords: EOT, DeepMIP, IODP, BAYSPLINE, BAYSPAR, BAYMBT

1. Introduction

The Eocene-Oligocene Transition (EOT) spans 34.4 to 33.7 Ma (Coxall & Pearson, 2007; Hutchinson et al., 2021; Katz et al., 2008) and marks the growth of permanent ice sheets on Antarctica (McKay et al., 2022). This transition includes a two-step increase in benthic foraminiferal ^{18}O by 1.5‰ (Coxall et al., 2005). The first step, the Earliest Oligocene Isotope Step (Hutchinson et al., 2021), increases by 0.7‰ denoting the expansion of the Antarctic ice sheet. Estimates for the size of the ice sheet based on the benthic ^{18}O signal suggest an ice sheet 60-130% of the modern East Antarctic Ice Sheet (Bohaty et al., 2012b; Lear et al., 2008). This transition is noted by a decrease in pCO_2 (Rae et al., 2021), temperature (Coxall & Pearson, 2007; Hutchinson et al., 2021; Lear et al., 2008; Liu et al., 2009), and sea level (Houben et al., 2012; Miller et al., 2020). An early hypothesis for the growth of permanent ice sheets on Antarctica was that gateway openings at the Drake Passage and Tasman Gateway led to thermal isolation of Antarctica (Kennett, 1977). Several ocean-only or intermediate complexity climate models suggest that the opening or deepening of the Southern Ocean gateways could have a local cooling effect close to the Antarctic coast (Sauermilch et al., 2021; Sijp et al., 2009). However, the accumulating proxy records and coupled climate modelling experiments have indicated that the gateway hypothesis does not fully explain the global cooling experienced at the EOT (e.g., Hutchinson et al., 2021). Ocean circulation proxy reconstructions indicate that the timing doesn't match the proposed mechanism. Deep water currents through the Tasman Gateway were first established around 30 Ma (Scher et al., 2015), i.e., after the EOT. For the Drake Passage, full opening may have occurred even later, in the Miocene (Dalziel et al., 2013).

A growing consensus is that a decrease in pCO_2 across the EOT is the primary driver for the EOT and temperature decrease globally (DeConto & Pollard, 2003; Goldner et al., 2014; Hutchinson et al., 2021; Lauretano et al., 2021; Pagani et al., 2011). Previous model proxy comparisons indicating a decrease in pCO_2 by 40% can explain the global temperature shift (Hutchinson et al., 2021). Recent pCO_2 compilations (Rae et al., 2021) constrain a decrease in pCO_2 from 980 to 830 ppmv from boron isotopes (16% decrease) (Anagnostou et al., 2016, 2020; Henehan et al., 2020; Pearson et al., 2009) and a decrease from 660 to 520 ppmv from alkenones (27% decreases) across the EOT (Pagani et al., 2005, 2011). Both proxies converge on the magnitude of the decrease being just 140-150 ppmv between the late Eocene and the early Oligocene, and when averaging across both proxies there is roughly a 25% decrease across the Eocene-Oligocene transition (Rae et al., 2021). Although carbon dioxide has been

established as the leading cause, additional feedbacks are invoked from both the ice-albedo feedback and gateway-induced changes to deep-water formation (Goldner et al., 2014). Several coupled climate model studies have found a shift from South Atlantic to South Pacific deep-water formation across the EOT due to Southern Ocean gateway opening (Kennedy et al., 2015; Toumoulin et al., 2020). Furthermore, deep water circulation proxies suggest that there was an expansion of North Atlantic Deep Water formation around the EOT (Coxall et al., 2018), supported by paleogeographic and modelling evidence of the Arctic becoming isolated from the North Atlantic (Hutchinson et al., 2019; Vahlenkamp et al., 2018). These studies suggest that ocean gateway and ice sheet changes could be involved in driving the observed changes at the EOT, although declining pCO_2 is the only mechanism proven to cause global cooling.

Climate models allow the drivers of change to be tested. Inter-model differences in boundary conditions (e.g., continental configuration) and parameterization schemes can lead to different outcomes. Multi-model comparisons can test the robustness of hypotheses for the transition to these differences in model formulation. One surprising feature of climate model experiments, is the finding of a smaller decrease in surface air temperatures at higher latitudes in comparison to mid-latitudes across the EOT (Kennedy-Asser et al., 2020). Model experiments also indicate Southern Ocean sea surface temperatures (SSTs) cooled more than the land at the same latitude. SST proxies indicate a global average cooling of 2.5°C across the EOT and regional differences in cooling ranging from 0 to 8°C (Hutchinson et al., 2021). Compiled global land surface mean air temperature (MAT) proxy records suggest a global mean cooling of 2.3°C with latitudinal and regional differences in cooling from 0 to 8°C (Hutchinson et al., 2021). However, proxy records are concentrated in northern mid-latitudes with limited records from the Southern Hemisphere and few from Antarctica. The sparse coverage of proxy records in the Southern Hemisphere and from Antarctica has hampered past efforts to evaluate model outputs.

We now have more temperature records to assess the magnitude of the land and sea temperature shift across the EOT surrounding the Southern Ocean. For example, there are now *br*GDGT-based temperature estimates on both sides of the Southern Ocean from Prydz Bay (Tibbett et al., 2021) and South Australia (Lauretano et al., 2021). We add these new records to compiled proxies and model experiments for the EOT (compiled by Hutchinson et al., 2021). That study compiled proxy data globally, whereas we take a more in-depth look at the southern high latitudes (>45^{o}S) and Antarctica for this proxy-model comparison. While the individual model experiments generally used a halving of carbon dioxide to force a large EOT response, we scale the model experiments to identify the pCO_2 forcing required to better reproduce the temperature anomaly across the transition observed in the proxy data in the high southern latitudes. The focused proxy-model comparison allows us to identify differences within regions in the proxies and in the climate model experiments to reach new understanding of the forcing and response during the Eocene to Oligocene Transition on Antarctica and in the Southern Ocean region.

1. **Methods**

(a) **Proxy data**

Proxy temperature records were collected south of 45°S based on paleolatitudes for the late Eocene (40 to 34 Ma) and early Oligocene (34 to 30 Ma) collating records from land and sea for MAT and SST (**Figure 1**). Proxy methods for the temperature reconstructions are noted and where appropriate the data was recalibrated to the latest methods for compatibility within the compilation. Averaging may attenuate the magnitude of the abrupt changes in some cases where a rebound in temperature occurs post-EOT (Bohaty et al., 2012a; Tibbett et al., 2021). At Prydz Bay, cooling at the EOT was reported to be 4°C and 5°C for SST and MAT respectively (Tibbett et al., 2021), but by averaging across the Eocene and Oligocene timeslices defined here, the Oligocene-Eocene cooling is 2.2°C and 3.2°C for SST and MAT respectively. The effect of the timeslice average dampens the calculated cooling by 30-45%.

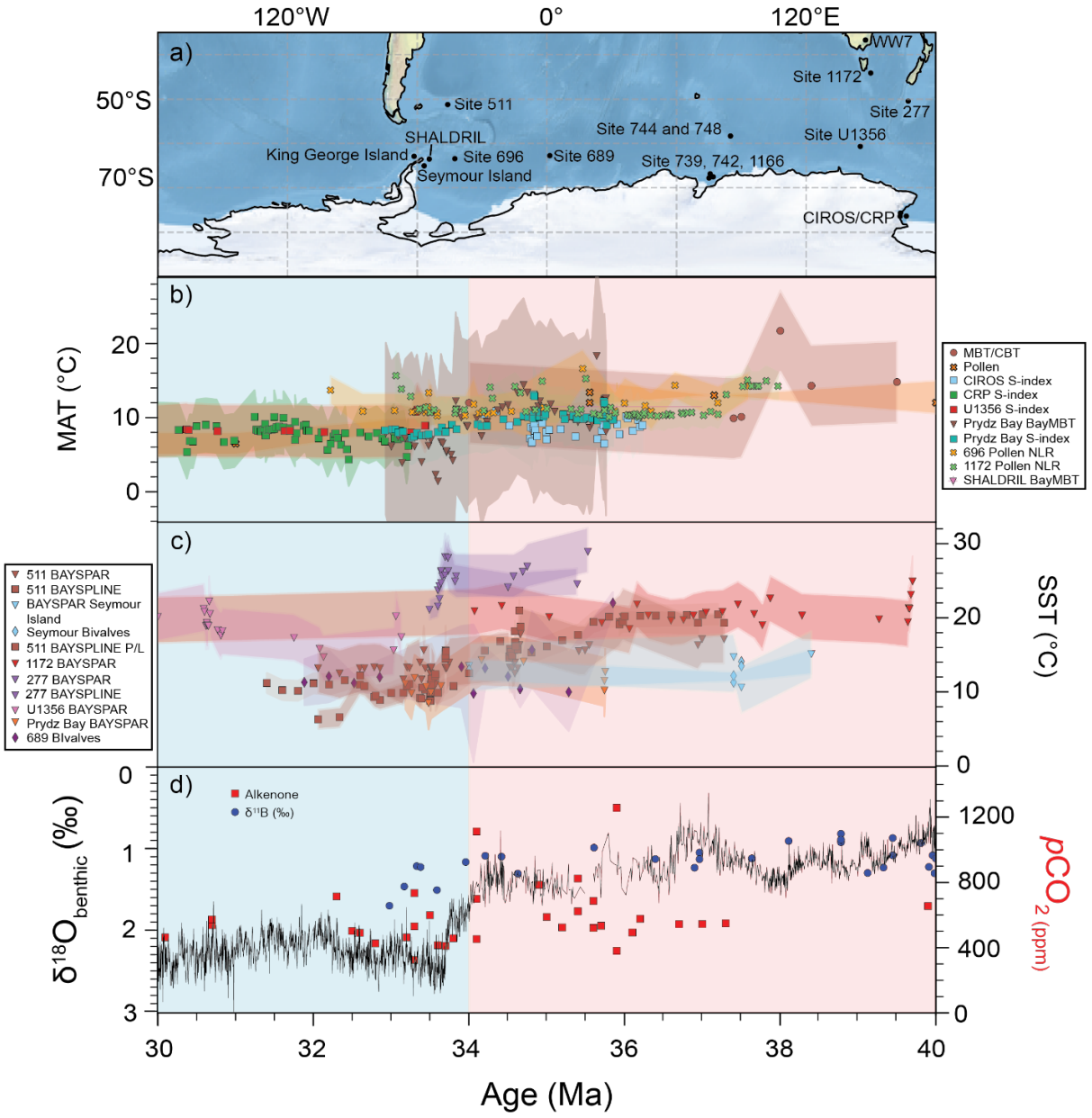

Figure 1. Proxy data compiled for Antarctica, the Southern Ocean and the southern high latitudes spanning the Eocene and Oligocene. a) Map depicting location of records used in this study. b) Land surface mean air temperature (MAT) data including BayMBT (Tibbett et al., 2021, 2022), pollen (Amoo et

al., 2022; Francis et al., 2008; Macphail & Truswell, 2004; Passchier et al., 2013; Poole et al., 2005; Thompson et al., 2022; Truswell & Macphail, 2009), S-index (Passchier et al., 2013, 2017), and MBT/CBT (Douglas et al., 2014). c) Sea surface temperature (SST) data from BAYSPAR calibrated TEX_{86} data (Douglas et al., 2014; Hartman et al., 2018; Houben et al., 2019; Lauretano et al., 2021; Pagani et al., 2011), SSTs from BAYSPLINE calibrated $U^{k'}{}_{37}$ (Houben et al., 2019; Liu et al., 2009; Pagani et al., 2011; Plancq et al., 2014), and Δ_{47} from bivalves (Douglas et al., 2014; Petersen & Schrag, 2015). d) $^{18}O_{benthic}$ spline (Westerhold et al., 2020) and pCO_2 compiled from ^{11}B (blue) and alkenone (red) proxies (Rae et al., 2021).

For the southern continents, reconstructions of mean annual air temperatures (MAT, **Table 1**) come from pollen assemblages (Amoo et al., 2022; Francis et al., 2008; Hunt & Poole, 2003; Macphail & Truswell, 2004; Poole et al., 2005; Thompson et al., 2022; Truswell & Macphail, 2009), the bacterial biomarker proxy indices of the branched Glycerol Dialkyl Glycerol Tetraethers (*br*GDGTs) with the more recent BayMBT (Bayesian regression model of the Methylation of Branched Tetraethers index) (Lauretano et al., 2021; Tibbett et al., 2021) and the earlier MBT/CBT (Cyclization of Branched Tetraethers) (Douglas et al., 2014), as well as mineral weathering via the S-index (Passchier et al., 2013, 2017). BayMBT are reported with the calibration to mean annual air temperature (Dearing Crampton-Flood et al., 2020) for the purposes of consistency with other mean annual air temperature (MAT) proxies and the reporting conventions for proxy-model comparison. However we will return to the seasonal question and the latest calibrations to months above freezing (MAF) based on the understanding that soil microbial communities are unlikely to be active below freezing (Deng et al., 2016; Weijers et al., 2007, 2011), at the end of the discussion. For both the Eocene and the Oligocene cases MAF approximates mean annual air temperature. An older proxy index of the *br*GDGT molecules, the MBT/CBT record cannot be recalibrated due to the lack of separation of the 5 and 6 methyl isomers with the laboratory methods in use at that time. We also have once instance of the peat-based estimate (Lauretano et al., 2021) using the MBT_{peat} calibration (Naafs et al., 2017).

Table 1. Mean annual air temperature proxy compilation for the Eocene and Oligocene.

Location	Lat	Long	Proxy	Eocene MAT (ºC)	Eocene standard deviation (ºC)	Oligocene MAT (ºC)	Oligocene standard deviation (ºC)	Oligocene-Eocene (ºC)	Reference
739, 742,1166	-67.3	75.1	BayMBT	11.0	2.0	6.8	2.6	-3.2	Tibbett et al., 2021
739, 742,1166	-67.3	75.1	S-index	10.4	1.0	8.1	0.5	-2.3	Passchier et al., 2017
CIROS-1 CRP Sites 2/3	-77.7	163.5	S-index	8.5	1.2	7.8	1.2	-0.7	Passchier et al., 2013
U1356	-63.3	136.0	S-index			8.9	1.2		Passchier et al., 2013
WW7	-38.2	147.1	MBT_{peat}	23.2	1.8	20.0	1.2	-3.2	Lauretano et al., 2021
Seymour Island	-64.4	-56.8	MBT/CBT*	13.8	4.4				Douglas et al., 2014
King George Island, Dragon Glacier	-62.1	-58.9	Pollen**	12.0					Poole et al., 2005, Hunt and Poole et al., 2003
King George Island, Fossil Hill	-62.1	-58.9	Pollen**	13.3					Poole et al., 2005
McMurdo	-77.6	166.4	Pollen**	13.0					Francis et al., 2009, p.331
King George Island, South Sheltand Island	-62.0	-58.4	Pollen**	13.4					Francis et al., 2009, p.326
1166	-67.3	75.1	Pollen**	12.0					Macphail and Truswell, 2004; Truswell and Macphail, 2009
CRP-3	-77.0	163.7	Pollen**			6.5			Francis et al., 2009, p.331
SHALDRIL	-63.8	-54.7	BayMBT	6.9	0.5				Tibbett et al., 2022
696	-61.8	-42.9	Pollen	11.9	1.8	11.2	1.0	-0.7	Thompson et al., 2022
1172	-43.9	158.3	Pollen	11.7	1.7	11.9	1.7	+0.2	Amoo et al., 2022

* Douglas et al., (2014) also reported MBT /CBT, excluded as unrealistically warm. **Pollen-based temperature estimates are reported here as MAT. Standard deviations represent timeseries variability. Latitude and longitude are reported for the present and are reported to 0.1° resolution

Southern Ocean and other southern high latitude SST records (**Table 2**) derive from the archaeal membrane lipid TEX_{86} index (Douglas et al., 2014; Hartman et al., 2018; Lauretano et al., 2021; Tibbett et al., 2021), the haptophyte algal biomarker $U^{k'}_{37}$ index (Houben et al., 2019; Liu et al., 2009; Pagani et al., 2011; Plancq et al., 2014) produced by the Reticulofenestrids in the Eocene and Oligocene (Henderiks & Pagani, 2008) and carbonates with temperatures derived from clumped isotopes Δ_{47} values measured on shallow coastal bivalves (Douglas et al., 2014; Petersen & Schrag, 2015), and ^{18}O value of planktonic foraminifera (Zachos et al., 1994). For Douglas et al., 2014 the TEX_{86} SSTs were reevaluated using BAYSPAR (Bayesian, Spatially-Varying Regression calibration for TEX_{86}) (Tierney & Tingley, 2014) with a prior of 13°C and a standard deviation of 15°C. Other TEX_{86} records from the Southern Ocean were either

originally calibrated by BAYSPAR (Hartman et al., 2018; Lauretano et al., 2021; Tibbett et al., 2021), or were recently reevaluated using BAYSPAR (Lauretano et al., 2021) with priors ranging from 12 to 21°C and a standard deviation of 20°C. The $U^{k'}_{37}$ records were reinterpreted using the latest BAYSPLINE (B-spline fit with a Bayesian regression) calibration (Tierney & Tingley, 2018)

Table 2. Sea surface temperature proxy compilation for the Eocene and Oligocene.

Site	Lat	Long	Proxy	Eocene SST (ºC)	Eocene standard deviation (ºC)	Oligocene SST (ºC)	Oligocene standard deviation (ºC)	Oligocene -Eocene (ºC)	Reference
739,742,1166	-67.3	75.1	BAYSPAR	12.6	1.7	10.4	1.1	-2.2	Tibbett et al., 2021
689	-64.5	-3.1	Δ_{47}	13.3	5.0	12.0	0.9	-1.1	Petersen and Schrag, 2015
744 and 748	-61.6	80.6	$\delta^{18}O$	6.0		5.0		-1.0	Zachos et al., 1994
689	-64.5	-3.1	$\delta^{18}O$	3.0		2.0		-1.0	Zachos et al., 1994
511	-51.0	-47.0	BAYSPAR	15.7	2.1	13.1	1.0	-2.6	Houben et al., 2019 updated with BAYSPAR from Lauretano et al., 2021
511	-51.0	-47.0	BAYSPLINE	17.6	2.1	10.8	2.5	-6.8	Houben et al., 2019*, updated with BAYSPLINE this ms**
511	-51.0	-47.0	BAYSPLINE	18.2	2.5	10.7	0.8	-7.5	Plancq et al., 2014; Liu et al., 2009, sourced from Elsworth et al., 2017 updated with BAYSPLINE this ms**
277	-52.2	166.2	BAYSPAR	26.9	1.4	25.8	1.4	-1.1	Lauretano et al., 2021 updated with BAYSPAR from Pagani et al., 2011
277	-52.2	166.2	BAYSPLINE	24.3	0.3	24.1	2.5	-0.2	Pagani et al., 2011, updated to BAYSPLINE this ms**
1172	-43.9	158.3	BAYSPAR	20.8	1.4	20.5	0.9	-0.3	Houben et al., 2019 updated with BAYSPAR from Lauretano et al., 2021
U1356	-63.3	136.0	BAYSPAR			18.7	2.0		Hartman et al., 2018
Seymour Island	-64.4	-56.8	BAYSPAR	13.5	2.1				Douglas et al., 2014, updated with BAYSPAR this ms
Seymour Island	-64.4	-56.8	Δ_{47}	12.9	0.7				Douglas et al., 2014

* DSDP Site 511 temperature reconstruction (Houben et al., 2019) updated with ages from Lauretano et al., (2021). Site 511 has two BAYSPLINE entries both

anomalous cooling compared to the BAYSPAR. ** $U^{k'}_{37}$ values recalibrated here with BAYSPLINE. Standard deviations represent timeseries variability. Latitude and longitude are reported for the present and are reported to 0.1° resolution

Proxy uncertainty ranges vary by proxy and is defined in the original calibration studies for each proxy, although the uncertainty is necessarily less well known in application to the past. For the GDGT-based proxies, SST and MAT values estimated by BAYSPAR and BayMBT respectively, carry one standard deviation calibration uncertainty ca. 4°C. For S-index the reported calibration standard deviation is 3.6°C (Sheldon et al., 2002). The $U^{k'}_{37}$ BAYSPLINE calibration carries a standard deviation of ca. 4°C (Tierney & Tingley, 2018). For clumped isotopes temperature standard deviation is 2.5°C (Douglas et al., 2014) and the standard error reported for the liner regression of MBT/CBT to temperature is 5.5°C (Weijers et al., 2011). Pollen temperatures generated from nearest living relative analysis are reported to have a standard deviation of 2 to 3°C (Amoo et al., 2022; Thompson et al., 2022). The approaches used to quantify uncertainty do vary between calibration approaches, with the error propagation captured rigorously in the bayesian calibrations, the advantage of that approach, and may be underreported in other cases.

The uncertainty around the central estimate for each timeslice is dependent upon the number of data points and the variability and length of the window chosen. For the intervals chosen here we report the standard deviation for each timeseries representing the variability around the means for each timeslice (**Table 1 and 2**). The selection of a longer time window can lead to more time averaging and thus dampening of the magnitude of the transition.

At sites with multi-proxy reconstructions, we can assess the magnitude of proxy-proxy discrepancy at each site and for each timeslice. For Prydz Bay the difference between two MAT proxies (S-index and BayMBT) is up to 4°C, likely at least in part due to inferred higher elevation sourcing of the rock-erosion proxy (S-index) and lower elevation sourcing of soil microbial biomarkers (Tibbett et al., 2021). Both DSDP Site 511 and Site 277 have a consistent SST proxy-proxy discrepancy between BAYSPAR and $U^{k'}_{37}$ of ~2°C. Although consistent their temperature difference between the Eocene and Oligocene varies with DSDP Site 511 cooling by ~3°C for BAYSPAR (Lauretano et al., 2021) and ~8°C after recalibrating $U^{k'}_{37}$ to BAYSPLINE (Houben et al., 2019). At Site 277 the cooling is more comparable ranging from 0.4 to 1.0°C (Lauretano et al., 2021; Pagani et al., 2011). Although both are reported and are used in this study as SSTs, haptophyte algae which produce alkenones (for the $U^{k'}_{37}$ index) are primary producers and are found in the photic zone (Popp et al., 2006; Volkman et al., 1980), whereas Thaumarchaeota (producers of *iso*GDGTs used for TEX_{86}) were more abundant in the subsurface of the Southern Ocean (Kalanetra et al., 2009), raising the possibility that proxy-proxy discrepancies may in part arise from different depth habitats when there is a vertical gradient in ocean temperatures.

1. **Models**

We re-use the ensemble of model experiments gathered onto a uniform grid by Hutchinson et al., (2021). The compiled experiments include two broad groupings 4x CO_2 (Eocene like) and 2x CO_2 (Oligocene like) each run without ice sheets to isolate only the effects of changing pCO_2 (**Table 3**). Additional model runs were included for a subset of models which included the paleogeography changes across the EOT (CESM_H, GFDL CM2.1, HadCM3BL, FOAM, UVic, NorESM-L), and the inclusion of an ice sheet (CESM_H, FOAM, HadCM3BL) (**Table 3**). While the NorESM-L model experiments run with a pCO_2 drop from 980 to 560 ppmv, this was scaled by Hutchinson et al., (2021) to match the 4x/2x simulations in the other models and applied here for consistency to compare the model temperature difference (O-E). The summary of the model parameters can be found in **Table 3** and detailed model run information for each of the models in the ensemble can be found in Hutchinson et al., (2021; and references therein). Here, we scale the model outputs to the proxy temperature differences to identify the pCO_2 decrease across the EOT as will be explained further in **Section 3.4**. Although commonly referred to as surface air temperature (SAT) in the model literature, in this manuscript we refer to land surface mean air temperatures as MAT throughout, to be consistent with the proxy literature.

Table 3. Model simulation parameters.

Model	pCO_2 runs (ppmv)	ice runs (volume km^3)	paleogeography runs	Reference	
	Eocene	Olig.	Eocene	Olig.	Eocene
CESM_B					
CESM_H			no ice	$20.3x10^6$	Drake and
FOAM			no ice	$25.0x10^6$	WA below
GFDL CM2.1					Arctic oper
HadCM3BL			no ice	$17.0x10^6$	Priabonian
NorESM-L	(980 initial)				Ma
UVic					Drake close

For models with more than one parameter all other factors held constant. NorESM-L was scaled to 1120 ppmv. For the ice/no ice runs pCO_2 is held constant at 560 ppmv. For the paleogeography runs the pCO_2 for both pre- and post-EOT is 1120 ppmv for CESM_H, 560 ppmv for FOAM, HadCM3BL and NorESM-L, 800 ppmv for GFDL CM2.1, and 1600 ppmv for UVic. Drake = Drake Passage, Tasman = Tasman Gateway, WA = West Antarctica, Olig = Oligocene.

Where land temperature proxies (e.g., soil bacterial biomarkers or soil weathering indicators) were recovered from marine sedimentary archives, we inferred

sourcing from the adjacent continent. Source regions were defined on the adjacent land mass, averaging the modelled surface temperatures within an area reflective of Antarctic drainage basins. For SST proxies we assume they capture temperatures in the overlying water column at the marine core site and thus compare to the nearest grid point within the model. In cases where marine archives appeared to plot "on land" due to modelled coastline imprecision, we obtained model comparison points from the nearest ocean grid cell for comparison to the marine core derived SST proxies. The proxy-model intercomparison differences are expressed as root mean square error (RMSE) (equation 1) with n as the number of proxies. This was assessed for each model scenario (Eocene and Oligocene) and the difference between the two.

$$RMSE = \sqrt{\frac{\sum_{i=1}^{n}(model-proxy)^2}{n}} \quad (1)$$

1. **Results**

   (a) **Proxy-model comparison**

      i. **pCO_2**

For the pCO_2 runs, the RMSE for the MAT ranges from 4.9 to 8.5°C for the Eocene, 6.5 to 9.4°C for the Oligocene, and 1.7 to 5.0°C for the difference comparison (**Figure 2 and Figure S1**). The RMSE for the SST ranges from 6.1 to 8.2°C for the Eocene, 6.7 to 8.8°C for the Oligocene, and 1.9 to 4.0°C for the temperature comparison (**Figure 3 and Figure S2**). The best fit for the Eocene data is CESM_B for both MAT and SSTs (4.9°C and 6.1°C) as well as for the Oligocene MATs (6.5°C) and for SSTs (6.1°C) although for the SSTs GFDL CM2.1 has the same RMSE (6.1°C). The lowest RMSE for the 2x-4x pCO_2 comparison comes from HadCM3BL of 1.7°C and 1.9°C for MAT and SSTs respectively. Although they have the best fit to the data this would imply a higher pCO_2 decrease given the difference between the Eocene and Oligocene runs is a halving of pCO_2. The ensemble mean RMSE, for a halving of pCO_2, is 2.7°C and 2.3°C for MATs and SSTs respectively.

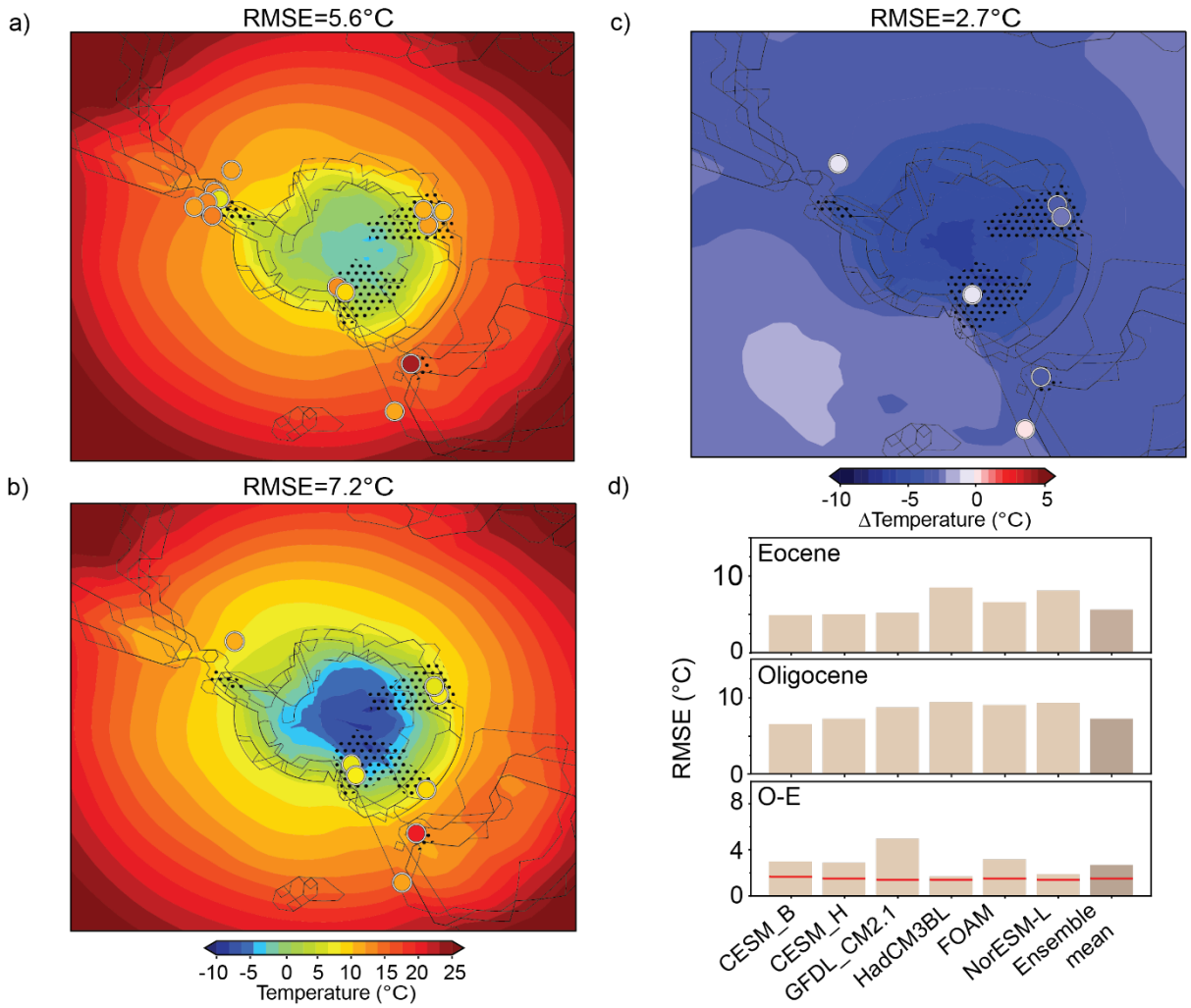

Figure 2. Southern hemisphere model MAT for the a) Eocene (4x pCO_2), b) Oligocene (2x pCO_2 model runs), and c) the difference across the transition (2x-4x) showing results for the unscaled multi model ensemble mean. The circles correspond to proxy mean annual air temperature records while the dotted areas show the source area used to compare the model temperature to the proxy record. d) The RMSE for pCO_2 model runs for MAT, for individual model mapped output see **Figure S1**. Red lines are the RMSE for each model after the pCO_2 scaling for RMSE values see **Table S1**.

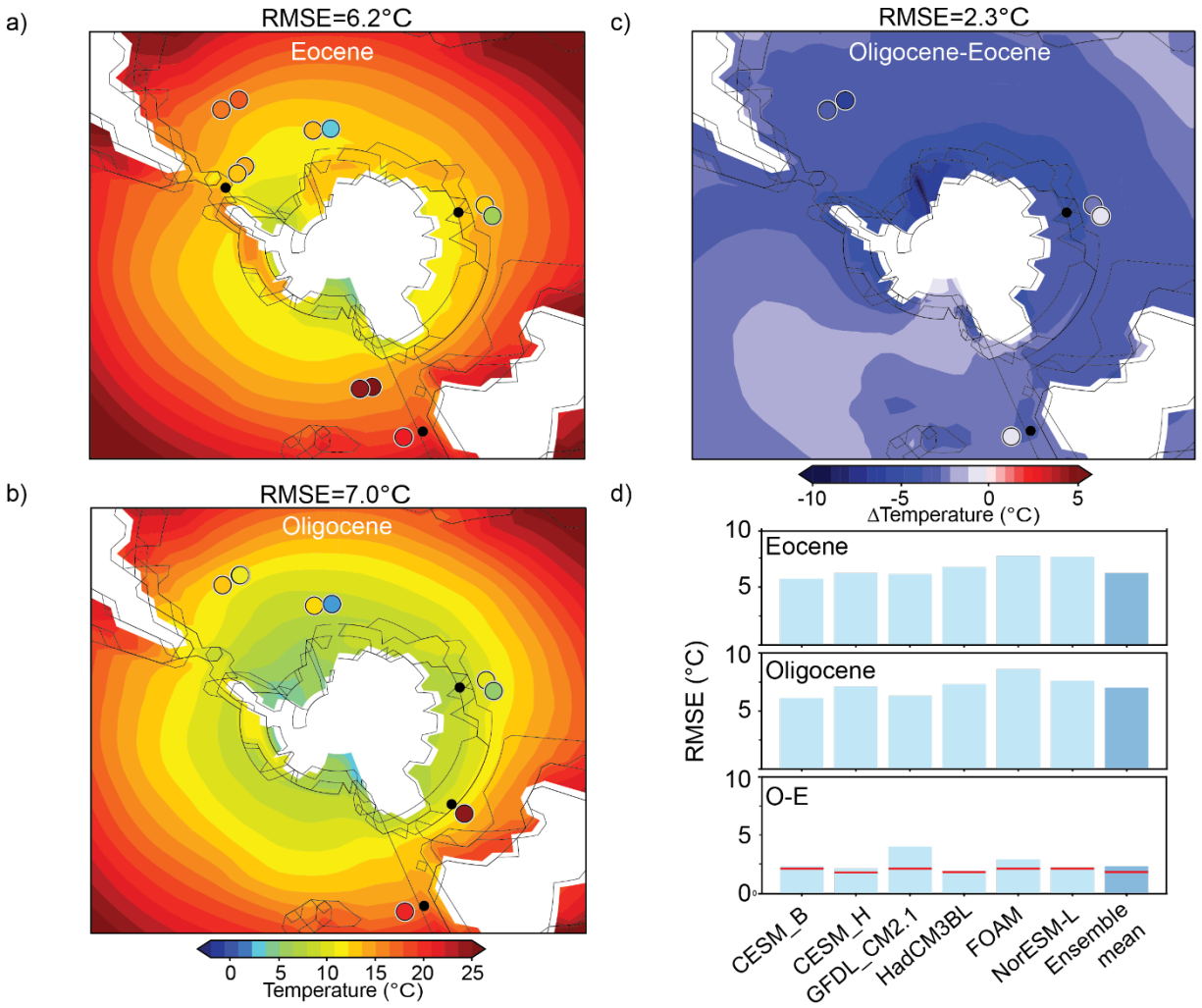

Figure 3. Southern Ocean sea surface temperatures (SST) for the a) Eocene (4x pCO_2), b) Oligocene (2x pCO_2 model runs), and c) the difference across the transition (2x-4x) showing results for the unscaled multi model ensemble mean. The circles correspond to proxy mean annual air temperature records while the dotted areas show the source area used to compare the model temperature to the proxy record. d) Summarizing the RMSE for pCO_2 model runs for SST, for individual model mapped output see **Figure S2**. Red lines are the RMSE for each model after the pCO_2 scaling for RMSE values see **Table S1**.

1. **Ice sheet**

For the ice sheet comparison only 3 models were used (CESM_H, HadCM3BL, and FOAM) as well as the ensemble mean. The RMSE for MAT ranged from 8.6 to 11.0°C for the Eocene, 18.3 to 24.7°C for the Oligocene, and 9.4 to 14.1°C for

the temperature comparison (**Figure 4 and Figure S3**). The RMSE for SST ranged from 7.9 to 9.3°C for the Eocene, 7.4 to 8.3°C for the Oligocene, and 2.4 to 2.8°C for the ice-no ice comparison (**Figure 4 and Figure S4**). The lowest RMSE for MAT comes from the HadCM3BL model and for SST the CESM_H model for the difference comparison. FOAM has the highest RMSE across all three time slices for SST. The Eocene MAT no ice runs have a higher RMSE (average of ~10°C when excluding the ensemble mean) compared to the MAT Eocene pCO_2 run RMSE (average of ~6°C excluding the ensemble mean) which are run at a higher pCO2 (800-1120 ppmv versus 560 ppmv for Eocene ice runs) indicating that a high pCO_2 is needed to better reflect Eocene temperatures. For the Oligocene there are substantial proxy-model discrepancies (high RMSE). Proxies confidently identify MAT above freezing, whereas the climate models forced with a large difference between the ice and no ice runs yields too large a cooling compared to proxies.

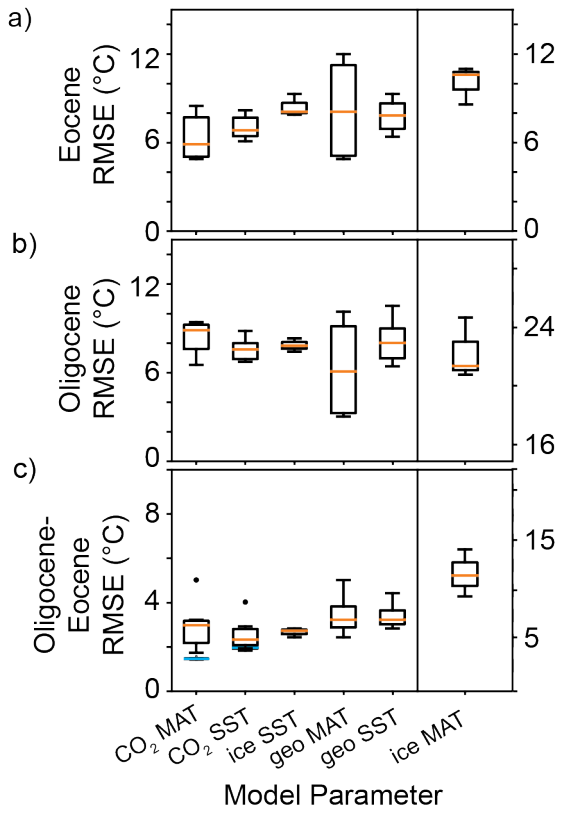

Figure 4. Summary of average RMSE across the model experiments a) Eocene runs for CO_2 using 4x pCO_2 (Table 3), ice runs contain no ice with pCO_2 of 560 ppmv, Eocene paleogeography runs (**Table 3**) b) Oligocene runs for pCO_2 using 2x pCO_2, ice runs containing the model prescribed ice sheet with pCO_2 of

560 ppmv, and Oligocene paleogeography runs (**Table 3**). Mean is the orange line with outliers as dots. Dots are outliers with both from the GFDL CM2.1 model. Blue line is the ensemble mean from the $p\mathrm{CO}_2$ scaling.

1. **Paleogeography**

Paleogeography was changed across all models except for CESM_B with $p\mathrm{CO}_2$ held constant between the Eocene and Oligocene runs. Both CESM_H, GDFL CM2.1, and UViC reflect changes in ocean gateways while FOAM represents West Antarctica being above sea level in the Eocene and mostly below sea level in the Oligocene representation **(Table 3**). NorESM-L and HadCM3BL model slight changes in continental positions from the Late Eocene to early Oligocene. The RMSE for MAT ranged from 4.9 to 12.0°C for the Eocene, 3.0 to 10.1°C for the Oligocene, and 2.4 to 5.0°C for the temperature comparison (**Figure 4 and Figure S5**). The RMSE for SST ranged from 6.4 to 9.3°C for the Eocene, 6.4 to 10.5°C for the Oligocene, and 2.8 to 4.4°C for the difference comparison (**Figure 4 and Figure S6**). The ensemble mean for MAT and SST is 3.0°C. For the Eocene MAT runs GFDL CM2.1 has the lowest RMSE of 5.2°C while for the Oligocene CESM_H has the lowest RMSE of 3.0°C. For the Eocene and Oligocene SST runs GFDL CM2.1 had the lowest RMSE of 6.4°C for the Eocene and UViC had the lowest RMSE of 6.4°C for the Oligocene. For the difference between the paleogeography for each model run the lowest RMSE was 2.4°C and 2.8°C from FOAM and UVic for MAT and FOAM for SST (**Figure S5 and S6**). The best fit to the Eocene data is from the model with the lowest $p\mathrm{CO}_2$ of 800 ppmv compared to the other models with $p\mathrm{CO}_2$ of 1120 ppmv and 1600 ppmv for UVic. Most of the models suggest a warming in MAT with regional differences (**Figure S5**). This in contrast to the proxy data which suggest temperature changes of 0 to -3°C. The model with the best fit for post/pre paleogeography is FOAM which has the most cooling regionally. To note additional regional differences UVic indicates more warming in the Pacific and Ross Sea sectors of the Southern Ocean while CESM_H suggest warming in the Atlantic and Indian Ocean sector with a cooling in the Pacific and Ross Sea sectors. This difference could be attributed to the prescribed modeled gateway opening in the Southern Ocean with CESM_H modeling the opening of Drake Passage and the Tasman Gateway and UVic modeling the opening of only Drake Passage. The overall warming trend suggests that paleogeography is not the primary driver of hemispheric cooling as previously noted (Hutchinson et al., 2021; Kennedy-Asser et al., 2020) but could impact regional differences in combination with $p\mathrm{CO}_2$. It also remains plausible that paleogeography changes could have indirectly triggered $p\mathrm{CO}_2$ changes. Two such mechanisms include a shift in the dominant basin of deep-water formation changing the ocean's ability to store carbon (Fyke et al., 2015; Speelman et al., 2009), or through land-based CO_2 weathering feedbacks triggered by the onset of the Atlantic meridional overturning circulation (Elsworth et al., 2017).

1. **CO_2 scaling**

As in the approach of Hutchinson et al., (2021), $p\mathrm{CO}_2$ was scaled by a constant

to determine the forcing required to achieve the best fit between the proxies and the model for each model. Here we compare the updated Antarctic proxy record (rather than the global proxy data) with scaled $p\mathrm{CO}_2$ to both surface air temperature and sea surface temperature. For the $p\mathrm{CO}_2$ decrease calculations the assumed post-EOT $p\mathrm{CO}_2$ is set at 560 ppmv, since this matches most of the models. RMSE was calculated between the difference between the 2x-4x $p\mathrm{CO}_2$ runs and the Oligocene-Eocene proxies for both MAT and SST. By varying the scaling factor, we found the lowest RMSE and the best estimated decrease in $p\mathrm{CO}_2$ for each model for MAT and SST proxies separately (**Figure 5**, **Table S1**). Averaging across all models (excluding the model ensemble mean), the average $p\mathrm{CO}_2$ decrease is 199 ppmv for MAT and 342 ppmv for SST.

In order to achieve best fit to the proxy data, the largest decrease in $p\mathrm{CO}_2$ is required in the HadCM3BL (608 ppmv) and NorESM-L (485 ppmv) climate models when fitting to the proxy SST data. When fitting to the smaller MAT difference, commensurately smaller changes are needed, with the largest changes needed in the HadCM3BL (337 ppmv) and NorESM-L (289 ppmv) when matching the shift in MAT.

The lowest RMSE for MAT is 1.42°C and for SST it is 1.89°C for the NorESM-L and CESM_H/HadCM3BL model experiments respectively. Although the RMSE range is small ranging from 1.4 to 1.6°C for MAT and 1.9 to 2.1°C for SST. SSTs have the highest range in $p\mathrm{CO}_2$ percent decrease (22.1-46.4%) in comparison to the SATs (17.6 to 37.6°C) (**Table 3**). The ensemble mean indicates a decrease of $p\mathrm{CO}_2$ of 27.3 and 34.0% across the Eocene-Oligocene Transition for MAT and SST respectively.

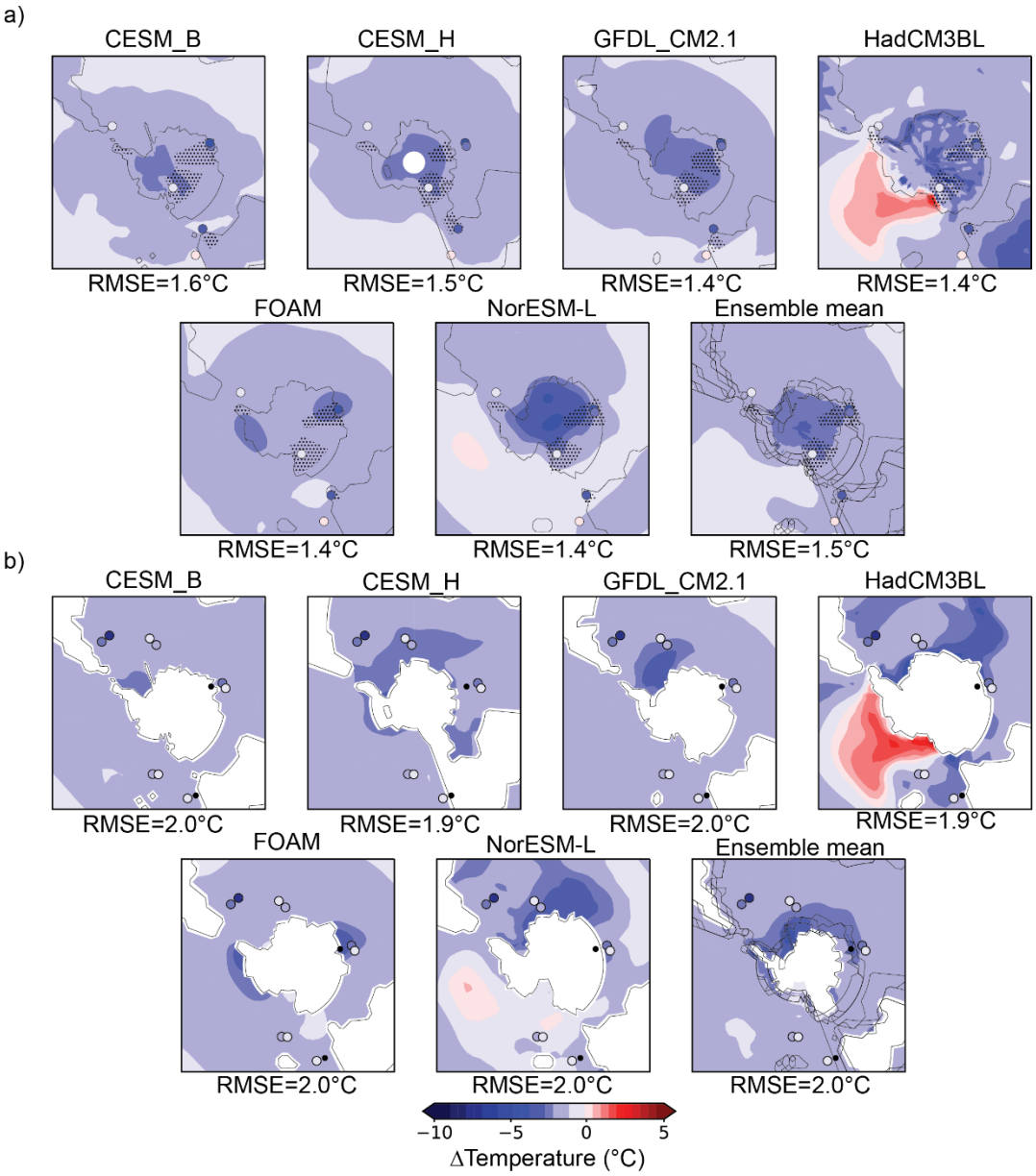

5. a) Proxy-model MAT comparison after scaling the pCO_2 forcing to achieve best fit to the magnitude of cooling in the proxy MATs, b) Proxy-model SST comparison after scaling the pCO_2 forcing to achieve best fit to the magnitude of cooling in the proxy SSTs.

1. **Discussion**

   (a) **Ice sheet extent**

The defining feature of the Eocene Oligocene Transition is the glaciation of Antarctica. The model runs used to represent the Oligocene in this comparison have prescribed ice sheet sizes ranging from 17x10^6, 20x10^6 , and 25 x10^6 km^3 for HadCM3BL, CESM_H, and FOAM respectively (Goldner et al., 2014; Kennedy et al., 2015; Ladant et al., 2014a; Ladant et al., 2014b). These ice volumes correspond to ~65%, 75% and 95% of the modern Antarctic ice sheet respectively, which fall within estimates from benthic ^{18}O that place the EAIS at 60-130% of the modern EAIS, with uncertainty due to the large range of estimates for $^{18}O_{ice}$ for the Oligocene (Bohaty et al., 2012b; Lear et al., 2008). However, climate model comparisons between ice and no ice runs yield too large a cooling for the EOT. Likely the ice sheet contrast imposed is too great (**Figure S3**), given that there was evidence for ephemeral Eocene glaciation, and unglaciated areas at the margins of the continent in the Oligocene as we review next.

The late Eocene included ephemeral glaciations notably the Priabonian Oxygen Isotope Maximum (PrOM) around ~37.5 Ma reaching the coastline, but not persisting (Scher et al., 2014), with glacial initiation in the Gamburtsev Mountains during the latest Eocene (Rose et al., 2013) and glacial erosion before the EOT (Carter et al., 2017; Galeotti et al., 2016). Geochemical evidence from the Kerguelen Plateau at 33.9-33.6 Ma (Scher et al., 2011), and sedimentary records from the western Ross Sea suggest the EOT glacial expansion reached the coast at 32.8 Ma (Galeotti et al., 2016). Modeling ice sheet growth found ephemeral glaciation when pCO_2 reached a threshold of 750-900 ppm (Van Breedam et al., 2022), these pCO_2 levels were reached during the late Eocene as far as back as 40 Ma based on pCO_2 reconstructions (**Figure 1c**) (Rae et al., 2021). Therefore, the lack of ice present in the late Eocene model runs does not match the available evidence for ephemeral ice in Antarctica and may contribute to the proxy-model temperature discrepancies for the individual timeslices.

After the EOT, the use of a full ice sheet for model outputs for the Oligocene is not consistent with pollen evidence for refugial vegetation on the Antarctic Peninsula (Anderson et al., 2011). Proxies record MAT above freezing in the Oligocene and the very presence of plants and soils bacteria indicates that an ice sheet did not cover the entire continent. The mismatch between reconstructed ice and the modelled ice/no ice scenario explains the large proxy-model RMSE for the EOT MATs (**Figure 4**).

We would also like to note that the ice sheet extent affects catchment sourcing. In this study, we defined source areas with basic polygons on the continent to represent the catchment area from which terrestrial proxies (e.g., soil biomarkers and rock weathering proxies) are exported to marginal marine settings. With the presence of a large ice sheet, soil and plant derived temperature proxies would be limited to unglaciated areas. However, detailed spatial ice sheet reconstructions are unavailable. Thus, for the purposes of this comparison, the source areas used in the model averaging were held constant for both the Eocene and Oligocene scenarios – a simplification given the likely range constriction following Oligocene glacial expansion.

1. **Southern Ocean**

SST proxies indicate cooling by an average of ~2°C across the EOT (**Table 2**). However, various proxies are used for the reconstructions which may lead to proxy-proxy disagreement (in particular at Site 511). The magnitude of the cooling also appears to differ spatially across the Southern Ocean (from 0 to 8 °C), which we will review by ocean sector as follows. These heterogenous proxy estimates are an impediment to model-proxy agreement at present (**Figure 5**).

In the Atlantic Ocean sector of the Southern Ocean, temperatures remain fairly constant from the Eocene to the Oligocene, for most of the records, with ~1°C cooling, well within proxy uncertainty (**Figure 3**). The largest cooling is recorded at DSDP Site 511, in the Atlantic Ocean sector of the Southern Ocean, where alkenone $U^{k'}_{37}$ evidence for an anomalous cooling of 8°C (Houben et al., 2019), contrasts with archaeal TEX_{86} BAYSPAR evidence for a cooling of 3°C (Lauretano et al., 2021), more in line with cooling elsewhere. At the same Site 511, dinocyst assemblages change from diverse, cosmopolitan species in the Eocene to high latitude endemics in the colder Oligocene (Houben et al., 2019). The larger estimated decrease in SSTs from the Atlantic sector Southern Ocean cooling is similar to estimates from a coupled climate model experiment, showing enhanced ocean overturning as deep water formation intensifies with cooling (Goldner et al., 2014).

In Prydz Bay, in the Indian Ocean sector of the Southern Ocean, SST using BAYSPAR cools by 2°C across the EOT (Tibbett et al., 2021). Further offshore at the Kerguelen Plateau SSTs drop by <1°C from ^{18}O (Zachos et al., 1994), consistent with expected differences between a near shore and open ocean site, although the same within uncertainties of the proxies. Given mean annual SSTs around 10°C in the Oligocene there was likely winter-season sea ice near the coast. Cooling is linked to sea ice development in Prydz Bay at the EOT (Hutchinson et al., 2018) and sea ice development has been predicted in climate models with Antarctic ice sheet forcing (Kennedy et al., 2015).

In the Pacific Ocean sector of the Southern Ocean, BAYSPAR and $U^{k'}_{37}$ proxies agree and both detect at most a 1°C change in SSTs from ODP Site 1172 (Houben et al., 2019) and DSDP Site 277 (Lauretano et al., 2021; Pagani et al., 2011). Similarly, some models have predicted little change or even warming SSTs in this area at ice sheet inception (Kennedy et al., 2015).

In almost all cases proxy-proxy agreement is good except at DSDP Site 511, on the Falkland Plateau, in the Atlantic Ocean, where the alkenone and archaeal SST proxies differ in the magnitude of the cooling. Elsewhere, in the sites surveyed here, these proxies agree thus there is likely no consistent proxy bias in terms of depth of production, seasonality or evolutionary changes not accounted for by calibration. Instead lateral advection of the alkenones is a likely explanation for offsets, and we note has previously led to the exclusion of data in this region from the modern datasets for the global calibration (Tierney & Tingley, 2018). Beyond the physical reasons for the offsets in the two proxies at Site 511,

that are necessarily inadequately constrained for the ancient ocean, we can evaluate the numerical implications of the proxy uncertainty. The experiment was rerun without the anomalous Site 511 alkenone data to identify how this would affect the comparison. The inclusion of alkenones at Site 511 with anomalously large cooling (~8°C) leads to a large proxy-model RMSE 1.97°C and leads to the largest calculated pCO_2 decrease across the EOT (34.0%), larger than proxy estimates. The exclusion of the anomalous cooling reconstructed by alkenones at Site 511 reduces the pCO_2 scaling to a 24.2% decrease in pCO_2, in line with proxy estimates (Rae et al., 2021) and the RMSE reduces to 0.71°C, making this the preferred choice. However, we note the low number of sites available (n=8) limits the robustness of this CO_2 scaling exercise overall.

1. **Declining pCO_2**

Based on the proxy-model comparison it is clear that the lowest RMSE for the Eocene occurs at higher pCO_2 (>560 ppmv) which is in line with previous estimates of pCO_2 suggesting a late Eocene pCO_2 of 830 to 980ppmv from boron and alkenone isotopes (Rae et al., 2021). Previous global proxy model comparison suggest a 40% decrease in pCO_2 across the EOT (Hutchinson et al., 2021), attributed to the lack of dynamic ice sheets and under sensitivity to CO_2 forcing (Hutchinson et al., 2021). The absolute pCO_2 levels are uncertain in the past, due to factors such as boron isotope seawater uncertainties; however, the boron isotope is better at assessing relative change (Raitzsch & Hönisch, 2013). The boron and alkenone isotopes are well studied for the EOT and have a high amount of data relative to other pCO_2 proxies. Current estimates of EOT pCO_2 changes from alkenone ^{13}C and boron isotopes suggest a decrease of 140 to 150 ppmv, or roughly 25% (Rae et al., 2021). The best fits between the proxies and model runs for the change in temperature, both MAT and SST, and across all the models (**Table 3 and Figure 5**) suggest a 18-38% decrease in pCO_2 for MAT and 15-38% decrease for SST after exclusion of Site 511 alkenone data. The percent decrease is similar to previous pCO_2 proxy estimates of 16% decrease from boron isotopes (Anagnostou et al., 2016, 2020; Henehan et al., 2020; Pearson et al., 2009) and a 27% decreases from alkenones (Pagani et al., 2005, 2011). The total amount (~210 ppmv) from the proxy-model comparison is within plausible range of proxy uncertainties. Given that the prescribed post-EOT level was 560 ppmv for the calculations the total amount may vary; however, the percent change is more comparable to pCO_2 records. The pCO_2 range falls within estimate from pCO_2 proxies. The discrepancy between the scaling and pCO_2 proxies could be due to additional forcing from ice-albedo feedbacks associated with from the presence of an ice sheet, sea ice (both likely) and/or changes in paleogeography.

1. **Accounting for proxy seasonality in proxy-model comparisons**

To assess the impact of seasonality on the proxy model comparison, we considered a seasonally-defined rather than mean annual comparison for land temperature proxies only. For land temperature proxies, both plants and soil bacteria are thought to be summer-active recorders, this motivates an effort to compare

to seasonal climate from the models. At this time, however, only BayMBT$_0$ has been explicitly calibrated to MAF, and only one site, Prydz Bay, has MAF estimates for both the Eocene and Oligocene. Using this MAF estimate and the other constraints as before, we compared to the climate model results and recalculated the pCO$_2$ scaling. The MAF proxy model comparison yields lower RMSE for the individual timeslices (**Figure S8, Table S2**). However, across the EOT the RMSE does not change and yields a similar estimated pCO$_2$ decrease (**Table S3 and Figure 6**). Although this seasonality proxy-model comparison is limited in application here, it demonstrates the potential for future work to calibrate proxies to seasons and to compare to the seasonal output of climate models in future efforts.

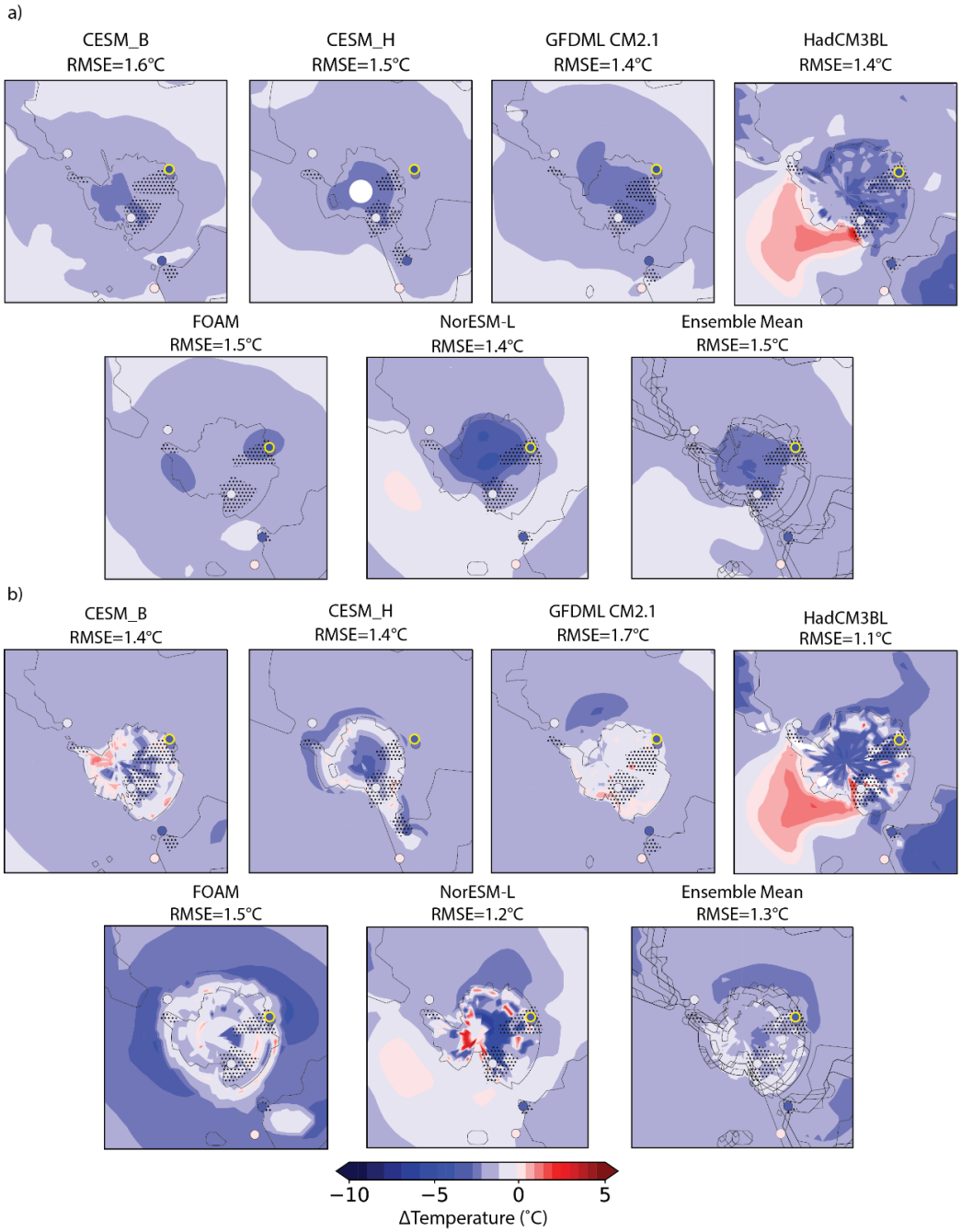

Figure 6. Best fit for pCO_2 across all models for a) MAT and b) MAF with

RMSE for each model and the ensemble mean. The yellow outline marks the proxy site that was recalibrated to MAF.

1. **Paleogeography with declining $p\mathbf{CO_2}$**

While the proxy evidence for SST change fits the expected $p\mathrm{CO}_2$ forcing across the Antarctic region, paleogeography could additionally affect regional patterns of cooling. To evaluate the effects of ocean gateways we used the three models with paleogeographic changes (UVic, CESM_H and FOAM) to derive a temperature anomaly due to gateway changes, denoted $\mathrm{T}_{\mathrm{GEOG}}$. Note, that $\mathrm{T}_{\mathrm{GEOG}}$ is calculate from individual models only, not an ensemble of the three models. For each model (UVic, CESM_H and FOAM), we combined this anomaly with the temperature anomaly due to $p\mathrm{CO}_2$ forcing (**Figure S9a**) from the whole ensemble, denoted $\mathrm{T}_{\mathrm{CO2}}$, and used adjustable scaling factors to find a temperature anomaly T to best fit to the proxy data:

$T = \alpha(T_{CO2} + T_{\mathrm{GEOG}})$ (2)

By scaling , we derive a decrease in $p\mathrm{CO}_2$ needed to best fit the proxy data (**Figure S9b, c, d, Table S4**). We excluded alkenone data from Site 511 which was anomalously cold as previously noted. The UVic model pre-EOT run has both the Drake Passage and Tasman Gateway closed while in the post-EOT run both the Drake Passage and Tasman Gateway are open. The CESM_H run model has the Tasman Gateway open post-EOT while the FOAM run models changes the surface area of West Antarctica. With the addition of the UVic model difference to the model ensemble mean $p\mathrm{CO}_2$ difference between the Oligocene and Eocene runs the decrease in $p\mathrm{CO}_2$ needed is 17.6% with an RMSE of 0.9. With the inclusion of CESM_H, the decrease in $p\mathrm{CO}_2$ is 21.0% with an RMSE of 0.88. With the inclusion of FOAM, the decrease in $p\mathrm{CO}_2$ is 15.3% with an RMSE of 0.97°C. The inclusion of the paleogeographic runs increases the ΔRMSE by 0.17 to 0.26°C, which is not significant. However, there is a clear change in the rescaled experiments in the amount of $p\mathrm{CO}_2$ needed to drive the transition. The lower $p\mathrm{CO}_2$ decrease, needed for the EOT with these model simulations, is consistent with the theory that the gateways opening around Antarctica were part of the explanation for the changes in regional SSTs.

1. **Sensitivity to proxy sampling density and model discrepancies**

In the EOT proxy-model comparison we acknowledge a limited number of SST and MAT proxy sites (<10 each) with most of the records clustered within a few regions of Antarctica. These limited spatial constraints affect the uncertainty. In theory, proxy-model comparisons could be improved with additional sites with proxy reconstructions. On the continent, the availability of additional archives is limited to sites with accessible, outcropping sediments of suitable age, and the modern ice cover is the main impediment. Geological field prospecting for available sediments is therefore the way to see what is possible in terms of adding more MAT estimates and a model-based approach would not be very fruitful to guide land sampling given accessibility limitations, although might help with prioritizing marine margin sites for terrestrial reconstruction. In the

open oceans, sediment is in theory deposited everywhere, though water depth and other conditions do limit the availability of SST proxies in some instances (whether through production or preservation). However, there remains great potential to add spatial coverage to proxy SST data and evaluate whether additional proxy records would decrease the proxy-model RMSE. Climate model experiments can help to target marine sampling efforts including guides to the optimal number and locations to drill. Here we demonstrate how an increasing number of sites can improve the uncertainty of proxy-model SST comparison RMSE, while also illuminating the existing model limitations through model-model comparisons.

To evaluate how additional marine core site SST and MAT reconstructions might affect the comparison with climate models, we performed a sensitivity test. First, we assigned one "perfect" model simulation as having the "true" temperature and using the same proxy sampling sites from the initial proxy-model comparison we compared to each of the other models to evaluate the error between models, by evaluating the estimated scaling factor with the assigned "true" temperature (**Table S5, Figure S10**). The individual models were able to estimate the 50% decrease in $p\mathrm{CO}_2$ within model runs and therefore we were able to recreate the same estimates between models. We then modeled the effect of adding all possible marine grid cells from 45°S to the Antarctic coastline for SST (n=710) and all possible land grid cells (n=960) from 60°S to 90°S for MAT comparisons. For most of the models the RMSE increased slightly between the initial model comparison with the prescribed proxy sites and the use of all the model grid cells. The ensemble mean increased from 1.04 to 1.42°C for MAT and 1.07 to 1.18°C for SST (**Fig S5**). Based on the minimal change in the RMSE from a low number of sites (n=6 MAT, n=9 SST) to the maximum number of grid cells (n=960 MAT, n=710 SST) it does not appear that the number of proxies is the limiting factor in this comparison. This suggests that the uncertainty in our proxy-model comparisons is primarily driven by discrepancies between the model simulations.

1. **Conclusions**

More paleoenvironmental proxy records are accumulating from the southern high latitudes allowing a new perspective on Antarctic-proximal changes across the EOT that were previously best known from records in the mid-latitudes of the Northern Hemisphere. These new records in the southern high latitudes highlight the spatially heterogeneous nature of cooling, with declines in SST (ranging from 0 to 8°C) and in MAT (0 to 3°C). However, proxy records are limited geographically, with no records spanning the late Eocene and early Oligocene from undersampled sectors of the Southern Ocean: the Bellingshausen and Amundsen Seas, or their adjacent landmasses. Climate model experiments with prescribed ice sheets lead to extreme local cooling in the Oligocene exceeding the proxy evidence for cooling. This comparison supports higher $p\mathrm{CO}_2$ estimates (>800 ppmv) for the late Eocene to match late Eocene temperature proxies. Here we compared proxy records to model outputs that assessed a de-

cline in pCO_2, changes in paleogeography, and the addition of a near or above modern size ice sheet. We use these various model experiments to estimate the decline in pCO_2 across the transition that provides the best fit to proxy records from the Antarctic across the Eocene-Oligocene Transition. The decline in MAT and SST from the new proxy compilation was used to scale model runs suggesting a 24-27% decrease in pCO_2 similar to recent pCO_2 compilations (Rae et al., 2021). This is encouraging as it suggests that the proxy and climate model data on temperature, pCO_2 and sensitivity may be converging on a coherent explanation for the magnitude of the pCO_2 forcing of the EOT. The SST proxy-model comparison identifies the need for an increase in proxy data coverage, better spanning longitudes to further constrain the uncertainties on the magnitude of the change, to assess proxy-proxy discrepancies, and to identify if paleogeography could explain the SST heterogeneity in the Southern Ocean. However, the lack of improvement when using additional grid cells for the model inter-comparison suggests that model disagreement is the major limiting factor in proxy-model comparisons here. While additional proxy records would increase the density of evidence for past climates, and these additional proxy data may improve the robustness of proxy-proxy comparisons, we show that this is not the main driver of the uncertainty (RMSE) in proxy-model comparisons at present. Our analysis identifies the primary source of uncertainty is within the model ensemble. The priority for future work is to address discrepancies in the temperature estimates among the model ensemble as well as the uncertainty surrounding estimation of the pCO_2 decrease needed to force the climate transition of the EOT.

Acknowledgements

We declare no financial conflicts of interests for any author or their affiliations. This research was funded by the U.S. National Science Foundation AGS-1844380 to NJB and OPP-1908548 to SJF. This work resulted from the GeoMeetsClimate MIP internship for EJT at GMU directed by NJB. DKH was supported by ARC grant DE220100279. Thanks to Scott Knapp for technical assistance to EJT with coding. Thanks to the various modeling and proxy groups that had made their data publicly accessible or fulfilled requests for data or metadata.

Data Availability Statement

The code used to perform the analysis and make the figures is available on GitHub (https://github.com/Ejtibbett/EOTproxymodel). The proxy compilation will be deposited into Zenodo before acceptance as it cannot be changed once submitted, we provide the proxy compilation as an Excel file for review.

References

Amoo, M., Salzmann, U., Pound, M. J., Thompson, N., & Bijl, P. K. (2022). Eocene to Oligocene vegetation and climate in the Tasmanian Gateway region were controlled by changes in ocean currents and pCO$_2$. *Climate of the Past*, *18*(3), 525–546. https://doi.org/10.5194/cp-18-525-2022Anagnostou, E., John, E. H., Babila, T. L., Sexton, P. F., Ridgwell, A., Lunt, D. J.,

Pearson, P. N., Chalk, T. B., Pancost, R. D., & Foster, G. L. (2020). Proxy evidence for state-dependence of climate sensitivity in the Eocene greenhouse. *Nature Communications*, *11*(1), 4436. https://doi.org/10.1038/s41467-020-17887-xAnagnostou, E., John, E. H., Edgar, K. M., Foster, G. L., Ridgwell, A., Inglis, G. N., Pancost, R. D., Lunt, D. J., & Pearson, P. N. (2016). Changing atmospheric CO2 concentration was the primary driver of early Cenozoic climate. *Nature*, *533*, 380.Baatsen, M., von der Heydt, A. S., Huber, M., Kliphuis, M. A., Bijl, P. K., Sluijs, A., & Dijkstra, H. A. (2020). The middle-to-late Eocene greenhouse climate, modelled using the CESM 1.0.5. *Climate of the Past Discussions*, *2020*, 1–44. https://doi.org/10.5194/cp-2020-29Bohaty, S. M., Zachos, J. C., & Delaney, M. L. (2012a). Foraminiferal Mg/Ca evidence for Southern Ocean cooling across the Eocene–Oligocene transition. *Earth and Planetary Science Letters*, *317–318*, 251–261. https://doi.org/10.1016/j.epsl.2011.11.037Bohaty, S. M., Zachos, J. C., & Delaney, M. L. (2012b). Foraminiferal Mg/Ca evidence for Southern Ocean cooling across the Eocene-Oligocene transition. *Earth and Planetary Science Letters*, *317*, 251–261. https://doi.org/10.1016/j.epsl.2011.11.037Carter, A., Riley, T. R., Hillenbrand, C.-D., & Rittner, M. (2017). Widespread Antarctic glaciation during the Late Eocene. *Earth and Planetary Science Letters*, *458*, 49–57. https://doi.org/10.1016/j.epsl.2016.10.045Coxall, H. K., Huck, C. E., Huber, M., Lear, C. H., Legarda-Lisarri, A., O'Regan, M., Sliwinska, K. K., van de Flierdt, T., de Boer, A. M., Zachos, J. C., & Backman, J. (2018). Export of nutrient rich Northern Component Water preceded early Oligocene Antarctic glaciation. *Nature Geoscience*, *11*(3), 190–196. https://doi.org/10.1038/s41561-018-0069-9Coxall, H. K., & Pearson, P. N. (2007). The Eocene-Oligocene transition. *Deep Time Perspectives on Climate Change: Marrying the Signal From Computer Models and Biological Proxies*, 351–387.Coxall, H. K., Wilson, P. A., Palike, H., Lear, C. H., & Backman, J. (2005). Rapid stepwise onset of Antarctic glaciation and deeper calcite compensation in the Pacific Ocean. *Nature*, *433*(7021), 53–57. https://doi.org/10.1038/nature03135Dalziel, I. W. D., Lawver, L. A., Pearce, J. A., Barker, P. F., Hastie, A. R., Barfod, D. N., Schenke, H.-W., & Davis, M. B. (2013). A potential barrier to deep Antarctic circumpolar flow until the late Miocene? *Geology*, *41*(9), 947–950. https://doi.org/10.1130/G34352.1Dearing Crampton-Flood, E., Tierney, J. E., Peterse, F., Kirkels, F. M. S. A., & Sinninghe Damsté, J. S. (2020). BayMBT: A Bayesian calibration model for branched glycerol dialkyl glycerol tetraethers in soils and peats. *Geochimica et Cosmochimica Acta*, *268*, 142–159. https://doi.org/10.1016/j.gca.2019.09.043DeConto, R. M., & Pollard, D. (2003). Rapid Cenozoic glaciation of Antarctica induced by declining atmospheric CO2. *Nature*, *421*(6920), 245–249. https://doi.org/10.1038/nature01290Deng, L., Jia, G., Jin, C., & Li, S. (2016). Warm season bias of branched GDGT temperature estimates causes underestimation of altitudinal lapse rate. *Organic Geochemistry*, *96*, 11–17. https://doi.org/10.1016/j.orggeochem.2016.03.004Douglas, P. M. J., Affek, H. P., Ivany, L. C., Houben, A. J. P., Sijp, W. P., Sluijs, A., Schouten, S., & Pagani, M. (2014). Pronounced zonal heterogeneity in Eocene southern

high-latitude sea surface temperatures. *Proceedings of the National Academy of Sciences*, *111*(18), 6582. https://doi.org/10.1073/pnas.1321441111Elsworth, G., Galbraith, E., Halverson, G., & Yang, S. (2017). Enhanced weathering and CO2 drawdown caused by latest Eocene strengthening of the Atlantic meridional overturning circulation. *Nature Geoscience*, *10*(3), 213–216. https://doi.org/10.1038/ngeo2888Francis, J. E., Marenssi, S., Levy, R., Hambrey, M., Thorn, V. C., Mohr, B., Brinkhuis, H., Warnaar, J., Zachos, J., Bohaty, S., & DeConto, R. (2008). Chapter 8 From Greenhouse to Icehouse – The Eocene/Oligocene in Antarctica. In F. Florindo & M. Siegert (Eds.), *Developments in Earth and Environmental Sciences* (Vol. 8, pp. 309–368). Elsevier. https://doi.org/10.1016/S1571-9197(08)00008-6Fyke, J. G., D'Orgeville, M., & Weaver, A. J. (2015). Drake Passage and Central American Seaway controls on the distribution of the oceanic carbon reservoir. *Global and Planetary Change*, *128*, 72–82. https://doi.org/10.1016/j.gloplacha.2015.02.011Galeotti, S., DeConto, R., Naish, T., Stocchi, P., Florindo, F., Pagani, M., Barrett, P., Bohaty, S. M., Lanci, L., Pollard, D., Sandroni, S., Talarico, F. M., & Zachos, J. C. (2016). Antarctic Ice Sheet variability across the Eocene-Oligocene boundary climate transition. *Science*, *352*(6281), 76. https://doi.org/10.1126/science.aab0669Goldner, A., Herold, N., & Huber, M. (2014). Antarctic glaciation caused ocean circulation changes at the Eocene–Oligocene transition. *Nature*, *511*(7511), 574–577. https://doi.org/10.1038/nature13597Hartman, J. D., Sangiorgi, F., Salabarnada, A., Peterse, F., Houben, A. J. P., Schouten, S., Brinkhuis, H., Escutia, C., & Bijl, P. K. (2018). Paleoceanography and ice sheet variability offshore Wilkes Land, Antarctica – Part 3: Insights from Oligocene–Miocene TEX_{86}-based sea surface temperature reconstructions. *Climate of the Past*, *14*(9), 1275–1297. https://doi.org/10.5194/cp-14-1275-2018Henderiks, J., & Pagani, M. (2008). Coccolithophore cell size and the Paleogene decline in atmospheric CO2. *Earth and Planetary Science Letters*, *269*(3), 576–584. https://doi.org/10.1016/j.epsl.2008.03.016Henehan, M. J., Edgar, K. M., Foster, G. L., Penman, D. E., Hull, P. M., Greenop, R., Anagnostou, E., & Pearson, P. N. (2020). Revisiting the Middle Eocene Climatic Optimum "Carbon Cycle Conundrum" with new estimates of atmospheric pCO2 from boron isotopes. *Paleoceanography and Paleoclimatology*, *35*(6), e2019PA003713.Houben, A. J. P., Bijl, P. K., Sluijs, A., Schouten, S., & Brinkhuis, H. (2019). Late Eocene Southern Ocean Cooling and Invigoration of Circulation Preconditioned Antarctica for Full-Scale Glaciation. *Geochemistry, Geophysics, Geosystems*, *20*(5), 2214–2234. https://doi.org/10.1029/2019GC008182Houben, A. J. P., van Mourik, C. A., Montanari, A., Coccioni, R., & Brinkhuis, H. (2012). The Eocene–Oligocene transition: Changes in sea level, temperature or both? *Cenozoic Evolution of Antarctic Climates, Oceans and Ice Sheets*, *335–336*, 75–83. https://doi.org/10.1016/j.palaeo.2011.04.008Hunt, R. J., & Poole, I. (2003). *Paleogene West Antarctic climate and vegetation history in light of new data from King George Island*.Hutchinson, D. K., Coxall, H. K., Lunt, D. J., Steinthorsdottir, M., de Boer, A. M., Baatsen, M., von der Heydt, A., Huber, M., Kennedy-Asser, A. T., Kunzmann, L.,

Ladant, J.-B., Lear, C. H., Moraweck, K., Pearson, P. N., Piga, E., Pound, M. J., Salzmann, U., Scher, H. D., Sijp, W. P., … Zhang, Z. (2021). The Eocene–Oligocene transition: A review of marine and terrestrial proxy data, models and model–data comparisons. *Climate of the Past*, *17*(1), 269–315. https://doi.org/10.5194/cp-17-269-2021Hutchinson, D. K., Coxall, H. K., O Regan, M., Nilsson, J., Caballero, R., & de Boer, A. M. (2019). Arctic closure as a trigger for Atlantic overturning at the Eocene-Oligocene Transition. *Nature Communications*, *10*(1), 3797. https://doi.org/10.1038/s41467-019-11828-zHutchinson, D. K., de Boer, A. M., Coxall, H. K., Caballero, R., Nilsson, J., & Baatsen, M. (2018). Climate sensitivity and meridional overturning circulation in the late Eocene using GFDL CM2.1. *Clim. Past*, *14*(6), 789–810. https://doi.org/10.5194/cp-14-789-2018Kalanetra, K. M., Bano, N., & Hollibaugh, J. T. (2009). Ammonia-oxidizing Archaea in the Arctic Ocean and Antarctic coastal waters. *Environmental Microbiology*, *11*(9), 2434–2445.Katz, M. E., Miller, K. G., Wright, J. D., Wade, B. S., Browning, J. V., Cramer, B. S., & Rosenthal, Y. (2008). Stepwise transition from the Eocene greenhouse to the Oligocene icehouse. *Nature Geoscience*, *1*(5), 329–334. https://doi.org/10.1038/ngeo179Kennedy, A. T., Farnsworth, A., Lunt, D. J., Lear, C. H., & Markwick, P. J. (2015). Atmospheric and oceanic impacts of Antarctic glaciation across the Eocene–Oligocene transition. *Philosophical Transactions of the Royal Society A: Mathematical, Physical and Engineering Sciences*, *373*(2054), 20140419. https://doi.org/10.1098/rsta.2014.0419Kennedy-Asser, A. T., Lunt, D. J., Valdes, P. J., Ladant, J.-B., Frieling, J., & Lauretano, V. (2020). Changes in the high-latitude Southern Hemisphere through the Eocene–Oligocene transition: A model–data comparison. *Climate of the Past*, *16*(2), 555–573. https://doi.org/10.5194/cp-16-555-2020Kennett, J. P. (1977). Cenozoic evolution of Antarctic glaciation, the circum-Antarctic Ocean, and their impact on global paleoceanography. *Journal of Geophysical Research (1896-1977)*, *82*(27), 3843–3860. https://doi.org/10.1029/JC082i027p03843Ladant, J.-B., Donnadieu, Y., & Dumas, C. (2014). Links between CO2, glaciation and water flow: Reconciling the Cenozoic history of the Antarctic Circumpolar Current. *Clim. Past*, *10*(6), 1957–1966. https://doi.org/10.5194/cp-10-1957-2014Ladant, J.-B., Donnadieu, Y., Lefebvre, V., & Dumas, C. (2014). The respective role of atmospheric carbon dioxide and orbital parameters on ice sheet evolution at the Eocene-Oligocene transition. *Paleoceanography*, *29*(8), 810–823. https://doi.org/10.1002/2013PA002593Lauretano, V., Kennedy-Asser, A. T., Korasidis, V. A., Wallace, M. W., Valdes, P. J., Lunt, D. J., Pancost, R. D., & Naafs, B. D. A. (2021). Eocene to Oligocene terrestrial Southern Hemisphere cooling caused by declining pCO2. *Nature Geoscience*, *14*(9), 659–664. https://doi.org/10.1038/s41561-021-00788-zLear, C. H., Bailey, T. R., Pearson, P. N., Coxall, H. K., & Rosenthal, Y. (2008). Cooling and ice growth across the Eocene-Oligocene transition. *Geology*, *36*(3), 251–254. https://doi.org/10.1130/G24584A.1Liu, Z., Pagani, M., Zinniker, D., DeConto, R., Huber, M., Brinkhuis, H., Shah, S. R., Leckie, R. M., & Pearson, A. (2009). Global Cooling During the Eocene-Oligocene Climate Transition.

Science, *323*(5918), 1187. https://doi.org/10.1126/science.1166368M. McKay, R., Escutia, C., De Santis, L., Donda, F., Duncan, B., Gohl, K., Gulick, S., Hernández-Molina, J., Hillenbrand, C.-D., Hochmuth, K., Kim, S., Kuhn, G., Larter, R., Leitchenkov, G., H. Levy, R., R. Naish, T., O'Brien, P., F. Pérez, L., E. Shevenell, A., & Williams, T. (2022). Chapter 3—Cenozoic history of Antarctic glaciation and climate from onshore and offshore studies. In F. Florindo, M. Siegert, L. D. Santis, & T. Naish (Eds.), *Antarctic Climate Evolution (Second Edition)* (pp. 41–164). Elsevier. https://doi.org/10.1016/B978-0-12-819109-5.00008-6Macphail, M. K., & Truswell, E. M. (2004). Palynology of Neogene slope and rise deposits from ODP Sites 1165 and 1167, East Antarctica. *Proceedings of the Ocean Drilling Program. Scientific Results*, *188*, 1–20.Miller, K. G., Browning, J. V., Schmelz, W. J., Kopp, R. E., Mountain, G. S., & Wright, J. D. (2020). Cenozoic sea-level and cryospheric evolution from deep-sea geochemical and continental margin records. *Science Advances*, *6*(20), eaaz1346. https://doi.org/10.1126/sciadv.aaz1346Naafs, B. D. A., Inglis, G. N., Zheng, Y., Amesbury, M. J., Biester, H., Bindler, R., Blewett, J., Burrows, M. A., del Castillo Torres, D., Chambers, F. M., Cohen, A. D., Evershed, R. P., Feakins, S. J., Gałka, M., Gallego-Sala, A., Gandois, L., Gray, D. M., Hatcher, P. G., Honorio Coronado, E. N., … Pancost, R. D. (2017). Introducing global peat-specific temperature and pH calibrations based on brGDGT bacterial lipids. *Geochimica et Cosmochimica Acta*, *208*, 285–301. https://doi.org/10.1016/j.gca.2017.01.038Pagani, M., Huber, M., Liu, Z., Bohaty, S. M., Henderiks, J., Sijp, W., Krishnan, S., & DeConto, R. M. (2011). The Role of Carbon Dioxide During the Onset of Antarctic Glaciation. *Science*, *334*(6060), 1261. https://doi.org/10.1126/science.1203909Pagani, M., Zachos, J. C., Freeman, K. H., Tipple, B., & Bohaty, S. (2005). Marked Decline in Atmospheric Carbon Dioxide Concentrations During the Paleogene. *Science*, *309*(5734), 600. https://doi.org/10.1126/science.1110063Passchier, S., Bohaty, S. M., Jimenez-Espejo, F. J., Pross, J., Roehl, U., van de Flierdt, T., Escutia, C., & Brinkhuis, H. (2013). Early Eocene to middle Miocene cooling and aridification of East Antarctica. *Geochemistry Geophysics Geosystems*, *14*(5), 1399–1410. https://doi.org/10.1002/ggge.20106Passchier, S., Ciarletta, D. J., Miriagos, T. E., Bijl, P. K., & Bohaty, S. M. (2017). An Antarctic stratigraphic record of stepwise ice growth through the Eocene-Oligocene transition. *Geological Society of America Bulletin*, *129*(3–4), 318–330. https://doi.org/10.1130/B31482.1Pearson, P. N., Foster, G. L., & Wade, B. S. (2009). Atmospheric carbon dioxide through the Eocene–Oligocene climate transition. *Nature*, *461*(7267), 1110–1113. https://doi.org/10.1038/nature08447Petersen, S. V., & Schrag, D. P. (2015). Antarctic ice growth before and after the Eocene-Oligocene transition: New estimates from clumped isotope paleothermometry: Antarctic ice growth at the E/O transition. *Paleoceanography*, *30*(10), 1305–1317. https://doi.org/10.1002/2014PA002769Plancq, J., Mattioli, E., Pittet, B., Simon, L., & Grossi, V. (2014). Productivity and sea-surface temperature changes recorded during the late Eocene–early Oligocene at DSDP Site 511 (South Atlantic). *Palaeogeography, Palaeoclimatology, Palaeoe-*

cology, *407*, 34–44. https://doi.org/10.1016/j.palaeo.2014.04.016Poole, I., Cantrill, D., & Utescher, T. (2005). A multi-proxy approach to determine Antarctic terrestrial palaeoclimate during the Late Cretaceous and Early Tertiary. *Palaeogeography, Palaeoclimatology, Palaeoecology*, *222*(1), 95–121. https://doi.org/10.1016/j.palaeo.2005.03.011Popp, B. N., Prahl, F. G., Wallsgrove, R. J., & Tanimoto, J. (2006). Seasonal patterns of alkenone production in the subtropical oligotrophic North Pacific. *Paleoceanography*, *21*(1). Scopus. https://doi.org/10.1029/2005PA001165Rae, J. W. B., Zhang, Y. G., Liu, X., Foster, G. L., Stoll, H. M., & Whiteford, R. D. M. (2021). Atmospheric CO2 over the Past 66 Million Years from Marine Archives. *Annual Review of Earth and Planetary Sciences*, *49*(1), 609–641. https://doi.org/10.1146/annurev-earth-082420-063026Raitzsch, M., & Hönisch, B. (2013). Cenozoic boron isotope variations in benthic foraminifers. *Geology*, *41*(5), 591–594. https://doi.org/10.1130/G34031.1Rose, K. C., Ferraccioli, F., Jamieson, S. S. R., Bell, R. E., Corr, H., Creyts, T. T., Braaten, D., Jordan, T. A., Fretwell, P. T., & Damaske, D. (2013). Early East Antarctic Ice Sheet growth recorded in the landscape of the Gamburtsev Subglacial Mountains. *Earth and Planetary Science Letters*, *375*, 1–12. https://doi.org/10.1016/j.epsl.2013.03.053Sauermilch, I., Whittaker, J. M., Klocker, A., Munday, D. R., Hochmuth, K., Bijl, P. K., & LaCasce, J. H. (2021). Gateway-driven weakening of ocean gyres leads to Southern Ocean cooling. *Nature Communications*, *12*(1), 6465. https://doi.org/10.1038/s41467-021-26658-1Scher, H. D., Bohaty, S. M., Smith, B. W., & Munn, G. H. (2014). Isotopic interrogation of a suspected late Eocene glaciation. *Paleoceanography*, *29*(6), 628–644. https://doi.org/10.1002/2014PA002648Scher, H. D., Bohaty, S. M., Zachos, J. C., & Delaney, M. L. (2011). Two-stepping into the icehouse: East Antarctic weathering during progressive ice-sheet expansion at the Eocene–Oligocene transition. *Geology*, *39*(4), 383–386. https://doi.org/10.1130/G31726.1Scher, H. D., Whittaker, J. M., Williams, S. E., Latimer, J. C., Kordesch, W. E. C., & Delaney, M. L. (2015). Onset of Antarctic Circumpolar Current 30 million years ago as Tasmanian Gateway aligned with westerlies. *Nature*, *523*(7562), 580–583. https://doi.org/10.1038/nature14598Sheldon, N. D., Retallack, G. J., & Tanaka, S. (2002). Geochemical Climofunctions from North American Soils and Application to Paleosols across the Eocene-Oligocene Boundary in Oregon. *The Journal of Geology*, *110*(6), 687–696. https://doi.org/10.1086/342865Sijp, W. P., England, M. H., & Toggweiler, J. R. (2009). Effect of Ocean Gateway Changes under Greenhouse Warmth. *Journal of Climate*, *22*(24), 6639–6652. https://doi.org/10.1175/2009JCLI3003.1Speelman, E. N., van Kempen, M. M., Barke, J., Brinkhuis, H., Reichart, G.-J., Smolders, A. J., Roelofs, J. G., Sangiorgi, F., de Leeuw, J. W., & Lotter, A. F. (2009). The Eocene Arctic Azolla bloom: Environmental conditions, productivity and carbon drawdown. *Geobiology*, *7*(2), 155–170.Thompson, N., Salzmann, U., López-Quirós, A., Bijl, P. K., Hoem, F. S., Etourneau, J., Sicre, M.-A., Roignant, S., Hocking, E., Amoo, M., & Escutia, C. (2022). Vegetation change across the Drake Passage region linked to late Eocene cooling and glacial disturbance after the Eocene–Oligocene

transition. *Climate of the Past*, *18*(2), 209–232. https://doi.org/10.5194/cp-18-209-2022Tibbett, E. J., Scher, H. D., Warny, S., Tierney, J. E., Passchier, S., & Feakins, S. J. (2021). Late Eocene Record of Hydrology and Temperature From Prydz Bay, East Antarctica. *Paleoceanography and Paleoclimatology*, *36*(4), e2020PA004204. https://doi.org/10.1029/2020PA004204Tibbett, E. J., Warny, S., Tierney, J. E., & Feakins, S. J. (2022). Cenozoic Antarctic Peninsula temperatures and glacial erosion signals from a multi-proxy biomarker study of SHALDRIL sediments. in review at *Paleoceanography and Paleoclimatology*. 2022PA004430Tierney, J. E., & Tingley, M. P. (2014). A Bayesian, spatially-varying calibration model for the TEX86 proxy. *Geochimica et Cosmochimica Acta*, *127*, 83–106.Tierney, J. E., & Tingley, M. P. (2018). BAYSPLINE: A New Calibration for the Alkenone Paleothermometer. *Paleoceanography and Paleoclimatology*, *33*(3), 281–301. https://doi.org/10.1002/2017PA003201Toumoulin, A., Donnadieu, Y., Ladant, J.-B., Batenburg, S. J., Poblete, F., & Dupont-Nivet, G. (2020). Quantifying the Effect of the Drake Passage Opening on the Eocene Ocean. *Paleoceanography and Paleoclimatology*, *35*(8), e2020PA003889. https://doi.org/10.1029/2020PA003889Truswell, E. M., & Macphail, M. K. (2009). Polar forests on the edge of extinction: What does the fossil spore and pollen evidence from East Antarctica say? *Australian Systematic Botany*, *22*(2), 57–106. https://doi.org/10.1071/SB08046Vahlenkamp, M., Niezgodzki, I., De Vleeschouwer, D., Lohmann, G., Bickert, T., & Pälike, H. (2018). Ocean and climate response to North Atlantic seaway changes at the onset of long-term Eocene cooling. *Earth and Planetary Science Letters*, *498*, 185–195. https://doi.org/10.1016/j.epsl.2018.06.031Van Breedam, J., Huybrechts, P., & Crucifix, M. (2022). Modelling evidence for late Eocene Antarctic glaciations. *Earth and Planetary Science Letters*, *586*, 117532. https://doi.org/10.1016/j.epsl.2022.117532Volkman, J. K., Eglinton, G., Corner, E. D. S., & Forsberg, T. E. V. (1980). Long-chain alkenes and alkenones in the marine coccolithophorid Emiliania huxleyi. *Phytochemistry*, *19*(12), 2619–2622. https://doi.org/10.1016/S0031-9422(00)83930-8Weijers, J. W. H., Bernhardt, B., Peterse, F., Werne, J. P., Dungait, J. A. J., Schouten, S., & Sinninghe Damsté, J. S. (2011). Absence of seasonal patterns in MBT–CBT indices in mid-latitude soils. *Geochimica et Cosmochimica Acta*, *75*(11), 3179–3190. https://doi.org/10.1016/j.gca.2011.03.015Weijers, J. W. H., Schouten, S., van den Donker, J. C., Hopmans, E. C., & Sinninghe Damsté, J. S. (2007). Environmental controls on bacterial tetraether membrane lipid distribution in soils. *Geochimica et Cosmochimica Acta*, *71*(3), 703–713. https://doi.org/10.1016/j.gca.2006.10.003Westerhold, T., Marwan, N., Drury, A. J., Liebrand, D., Agnini, C., Anagnostou, E., Barnet, J. S. K., Bohaty, S. M., Vleeschouwer, D. D., Florindo, F., Frederichs, T., Hodell, D. A., Holbourn, A. E., Kroon, D., Lauretano, V., Littler, K., Lourens, L. J., Lyle, M., Pälike, H., … Zachos, J. C. (2020). An astronomically dated record of Earth’s climate and its predictability over the last 66 million years. *Science*, *369*(6509), 1383–1387. https://doi.org/10.1126/science.aba6853Zachos, J. C., Stott, L. D., & Lohmann, K. C. (1994). Evolution of Early Cenozoic marine temperatures. *Paleoceanography*, *9*(2), 353–387. https://doi.org/10.1029/93PA03266